

## ORIGINAL RESEARCH

# Modulating sparks in a pulse train for repetitive and energy efficient plasma generation

 Bo Yin<sup>1</sup>  | Yifei Zhu<sup>1,2</sup> | Yun Wu<sup>1,3</sup>
<sup>1</sup>Institute of Aero-Engine, School of Mechanical Engineering, Xi'an Jiaotong University, Xi'an, China<sup>2</sup>School of Electrical Engineering, Xi'an Jiaotong University, Xi'an, China<sup>3</sup>Science and Technology of Plasma Dynamics Laboratory, Airforce Engineering University, Xi'an, China**Correspondence**
 Yifei Zhu and Yun Wu.  
 Email: [yifei.zhu.plasma@gmail.com](mailto:yifei.zhu.plasma@gmail.com) and  
[wuyun1223@126.com](mailto:wuyun1223@126.com)

Associate Editor: Yangyang Fu

**Funding information**
 National Natural Science Foundation of China,  
 Grant/Award Number: 51907204; Natural Science  
 Foundation of Shaanxi Province, Grant/Award  
 Number: 2021JQ-358
**Abstract**

Spark is a widely studied plasma source for active species production; however, it experiences unstable transitions (e.g. to a thermal arc) at high frequencies or long pulse durations. In this study, the sparks generated in a pulse train were studied and modulated based on a physics-corrected deep learning method. Our results show that a highly repeatable and stable spark plasma source can be achieved by automatically adjusting the voltage amplitude according to the discharge frequency in a high-frequency pulse train within the time scale of the fluid response. The influences of the electron number density increasing mode and modulated driven voltage profiles on the energy efficiencies were also studied.

## 1 | INTRODUCTION

Spark discharge plasma is generated between two bare electrodes. Streamers initiate and propagate towards the opposite electrode by applying a high-voltage pulse to one of the electrodes. Once the streamer penetrates the gas gap, a bright plasma channel connects the electrodes [1]. Compared with glow or streamer discharges, more energy can be deposited and more intensive gas heating is achieved in spark plasma. Compared with arc discharges, active species can produce more energy efficiently through the rich non-equilibrium chemical processes in spark plasma. The unique features of spark discharge plasma have attracted increasing attention from the community of ignition and combustion [2–5], flow control [6, 7], surface treatment [8–10], energy conversion [11–13], high-voltage switch design [14, 15], laser ignition [16, 17], and material engineering [18, 19].

Despite these advantages, the spark has long been considered as an ‘unstable’ plasma source in applications, as it stands in the middle of the non-equilibrium and equilibrium states. A spark, if not well modulated, can easily transform into

a thermal spark [20] in a few or tens or hundreds of nanoseconds, or conversely, periodically extinguish [21]. The heat release, high density of excited species, and high electric field trigger the aforementioned transitions, especially at high repetitive frequencies.

A repeatable and energy-efficient plasma source is preferred for industrial applications. Sparks generated by a pulse train could be promising plasma sources for highly efficient active species production and heating. By compressing a few or tens of pulses within the time scale of gas dynamics (a few microseconds in atmospheric pressure) in one periodic cycle (from microseconds to milliseconds), the influence of gas expansion on the reduced electric field (calculated from the electric field and the total species number density) can be avoided. By modulating each pulse in the train, it is possible to generate highly repeatable sparks and control the density of useful active species in each cycle in a smart/accurate and energy-efficient manner. An example of a high-frequency spark application can be found in recent publications on plasma jets driven by RF power sources [22–24].

This is an open access article under the terms of the [Creative Commons Attribution-NonCommercial-NoDerivs](https://creativecommons.org/licenses/by-nc-nd/4.0/) License, which permits use and distribution in any medium, provided the original work is properly cited, the use is non-commercial and no modifications or adaptations are made.

© 2023 The Authors. *High Voltage* published by John Wiley & Sons Ltd on behalf of The Institution of Engineering and Technology and China Electric Power Research Institute.

One of the challenges of smart spark generation in a pulse train is to design the profile of each pulse and automatically determine the relationship between the voltage pulse amplitude and frequency. This is an ‘inverse problem’: How can the pulse profile be determined to repeat the evolution of interesting species during the next pulse? The traditional design method based on experience or the ‘guess—test’ methodology is no longer suitable because of the highly non-linear process and complex chemistry with timescales ranging from a few nanoseconds to tens of microseconds.

Machine learning (ML) has exhibited significant potential for addressing problems in complex systems. The concept of Artificial Intelligence for Science has been proposed and implemented in gas dynamics [25, 26], combustion [27, 28], disease diagnosis [29, 30] and protein structure prediction [31, 32]. ML has also been used in plasma physics and applications, and some pioneering studies in the plasma science community can be found in refs. [33–38]. Van der Gaag et al. [39] used ML to inversely solve the bremsstrahlung emissivity equation. Kawaguchi et al. [40] used an artificial feed-forward neural network to solve Boltzmann’s equation for an electron velocity distribution function. Mesbah et al. [41] summarised the applications of ML in the modelling, diagnostics, and control of non-equilibrium plasma. In the field of ML-assisted plasma modelling, a double deep neural network (DNN) was developed and successively implemented to solve the partial differential equation systems of both thermal arc and low-temperature glow discharges [42, 43].

A physics-corrected plasma + deep learning framework, DeePlaskin, was developed and tested for non-equilibrium plasma systems [44]. The framework proposes a ‘predictor—corrector’ approach combining the DNN and a global model to reconstruct the temporal profile of the reduced electric field  $E/N$  (and thus the potential drop on the electrodes) based on pre-defined temporal evolution of target species.

In this study, we demonstrate how two successive sparks during one pulse train can be modulated using the DeePlaskin framework. The influence of the pulse frequency and increasing mode of the target species on the voltage pulse profiles are discussed. A two-dimensional (2D) code validated by experimental measurements was used to provide self-consistent inputs for the DeePlaskin framework. The remainder of this paper is organised as follows. The framework, 2D model, and coupling strategy are provided in section, the results and discussions are provided in section, and conclusions are drawn in section.

## 2 | MODEL AND METHODS

Three codes are used in a combined manner in this study: the ZDPlasKin code for plasma chemistry [45], PASSKEy code for plasma transport [46, 47], and DeePlasKin framework for inverse design [44].

### 2.1 | Discharge configuration and 2D self-consistent model

We considered the spark discharge configuration studied in ref [48] as a starting point: the gas pressure was 13,332.2 Pa, environmental temperature was 300 K, and discharge gas was air ( $N_2:O_2 = 4:1$ ). The anode was powered by a nanosecond pulsed generator, producing a 10 kV peak voltage during 100 ns at pulse repetition rates from 1 to 10 kHz. The geometry consisted of two spherical copper electrodes with a diameter of 7.5 mm, and the distance between the two electrodes was 10 mm. The geometry is shown in Figure 1a. The reason for this choice is that the low pressure and short pulse duration allow us to ignore the influence of gas heating and expansion on the short discharge timescale [49].

The discharge configuration was first calculated using 2D plasma code to provide self-consistent inputs for further analysis. The geometry and computational domain are shown in Figure 1b, the computational domain of the rectangle is  $35 \times 40$  mm, the red domain is the anode, the yellow is ground, and the blue is set as plasma domain. The 2D model was constructed to calculate the spatial-temporal evolution of the electric field, species densities, and fluid dynamics, and the Poisson equation, drift diffusion equations for electrons and ions, and three-Helmholtz equation model for photoionisation were solved together. Detailed numerical implementations can be found in previous studies [50]. The results calculated by the 2D code provide the electric field and initial electron density for the zero-dimensional (0D) model.

### 2.2 | Global chemistry model

The 0D global chemistry model was used to calculate the temporal evolution of species densities for detailed kinetics over a longtime scale, and generate a large amount of data for deep learning training. The 0D model starts once the ionisation wave passes the middle point ( $E/N$  reached its peak), and the plasma parameters ( $E/N$  and initial species densities) in the middle point of the 2D model (shown in Figure 2a,b) were selected to represent the entire channel. The initial time instant of the 0D model is determined by the moment when the ionisation front passes the fixed point of the discharge gap, to avoid the strong convection effect that offends against the homogeneous hypothesis of the 0D model. The reduced electric field calculated by the 2D model as the input of the 0D code is determined based on the ratio of the voltage to the electrode gap length.

The ZDPlasKin code, which embeds the BOLSIG+ [51] solver and QTPlaskin postprocessor, is used. The former is designed to calculate the electron reaction rate coefficients and electron energy distribution function, and the latter is used to read and view the output. A system of ordinary differential equations for time-dependent densities of the involved species during the period from 0 to 1000 ns was solved. The kinetic scheme of the air discharge was drawn from ref. [52], with 62 species (electrons,  $N_2$ ,  $O_2$ ,  $O$ ,  $O(^1D)$ ,  $O_3$ ,  $O^-$ ,  $O_3^-$ ,  $O_4^+$ ,  $N_2^+$ ,  $N_3^+$ ,  $N_2(C_3\Pi_u)$ ) and 718 chemical reactions. This scheme was

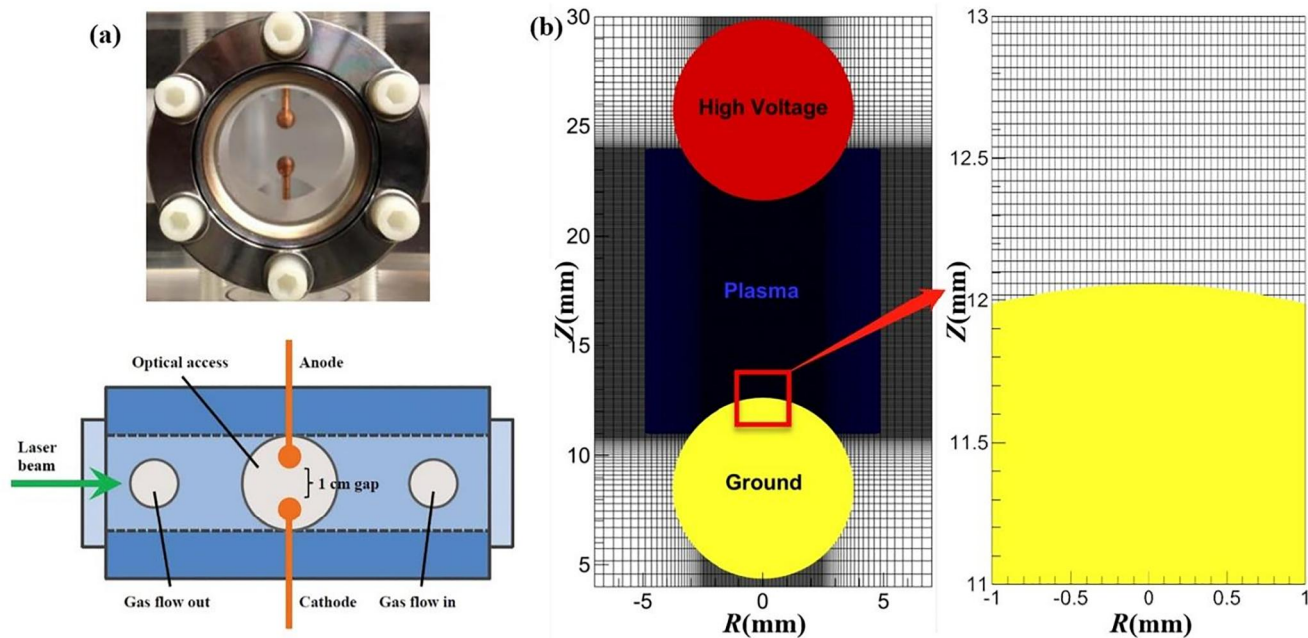


**FIGURE 1** The studied spark discharge configuration. (a) Photograph and schematic of the discharge cell in the experiment, extracted from ref. [48]. (b) Geometry and computational domain for 2D modelling.

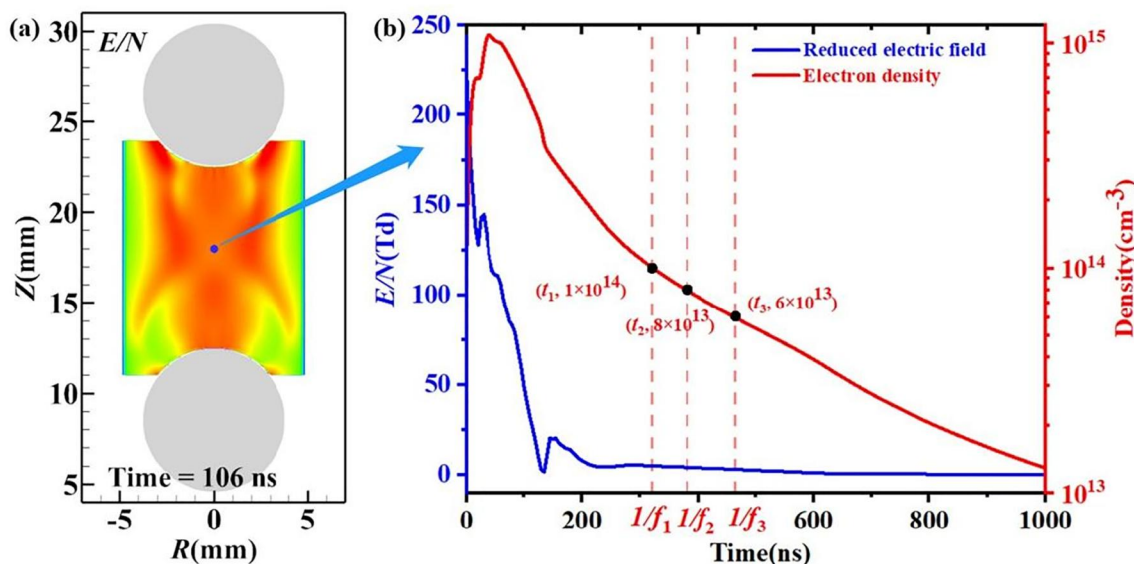


**FIGURE 2** (a) Distribution of  $E/N$  calculated by PASSKEy at the 106 ns. (b) Temporal evolution of the electron density calculated by ZDPlaskin at the middle point of the computational domain.

validated by optical emission spectroscopy experiments. The essence of the 0D chemistry model is to solve a set of first-order ordinary differential Equation (1).

$$\frac{d[N_i]}{dt} = f(E/N, n_{1,2,\dots}) \quad (1)$$

where  $N_i$  is the  $i$ th species density,  $dt$  is the time step, and  $n$  is the species density at the last time point.

To generate highly repeatable sparks and control the density of useful active species, three frequencies ( $f_1 = 1/t_1 = 3.12$  MHz,

$f_2 = 1/t_2 = 2.631$  MHz,  $f_3 = 1/t_3 = 2.15$  MHz) were selected to modulate the spark discharge, as shown in Figure 2b. In Section 3.2, the results for three different discharge frequencies are discussed.

### 2.3 | Deeplaskin framework

DeePlasKin combines the global plasma model and deep learning model to inversely solve the key parameters of



By trial and error, we chose a four-layer DNN to train the data, where the input and vector were 65 and 63 dimensions respectively. The input layer is used to receive the data and the output layer is the result. The hidden layers were used to learn the non-linear mapping relation between the input and output. The activation function is ReLU [53], using Equation (5) for each neuron.

$$f(x) = \max(0, x) \quad (5)$$

The ReLU is used to add non-linear factors to increase the expressiveness of the model such that it can compute gradients for non-linear functions faster. The loss function is the mean absolute function ( $M_{AE}$ ) obtained using Equation (6).

$$M_{AE} = \frac{\sum_{i=1}^n |y - \bar{y}|}{n} \quad (6)$$

where  $y$  is the predicted value and  $\bar{y}$  is the real value. The loss function is the difference between the predicted and real values. The task of ML is to minimise the loss function. Adam [54], whose job is to calculate the gradient of the loss function in each epoch and then update the weights and bias of neural networks to minimise the loss function, is used to solve the optimisation problem in this study. The training and validation errors for 200 epochs are shown in Figure 7b. The neural networks were implemented using tensorflow2.0 framework [55], an open-source ML library. After training, the model was used to predict the reduced electric field, and the predicted results were used to calculate the density of all species. If the difference between the calculated and predefined density values is larger than the tolerance, the code adjusts the predicted  $E/N$  to update the time and species densities according to physical laws. When the tolerance is met, the predicted reduced electric field and all species densities are outputted (to the 2D model for further validation).

## 2.4 | How the 2D model and the 0D global model couple with DeePlasKin

The 2D model, global plasma model, and DeePlasKin model are introduced, and the data exchange between them is shown in Figure 4. First, a 2D model was used to calculate the spatial-

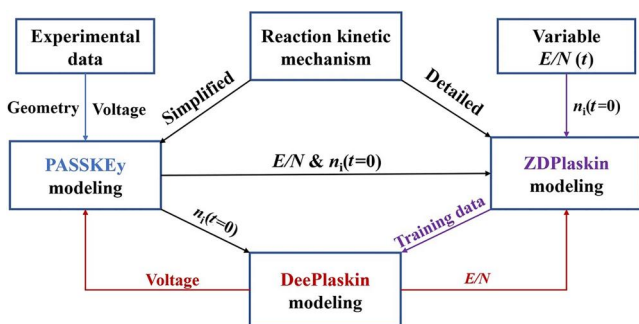


FIGURE 4 Data transfer between the DeePlasKin model, 0D model, and 2D model.

temporal evolution of the electric field, species densities, and fluid dynamics based on the experimental data. The 2D model provided the temporal evolution of  $E/N$  and the initial species densities to the 0D model to calculate the temporal evolution of species densities. The DeePlasKin model coupling the 0D model and deep learning model was used to reconstruct the waveform of the  $E/N$  based on the pre-defined temporal evolution of the target species. The voltage was then calculated according to the  $E/N$  reconstructed by DeePlasKin. The voltages were input into the 2D model to validate the spatial-temporal evolution of the electric field and species densities.

## 3 | RESULTS AND DISCUSSIONS

### 3.1 | Base case and validations

The spark discharge model was described in ref. [48] and the waveform of the applied voltage is shown in Figure 5a. The voltage was put into a 2D model to calculate the spatial-temporal evolution of the electric field and the distribution of species densities, and the calculated current and the distribution of the  $N_2(C_3\Pi_u)$  density were in good agreement with the experiment in Figure 5a,b. The streamer propagation stage is shown in Figure 6, where (a1)–(a5) and (b1)–(b5) are the spatial-temporal evolution of the electron density and reduced electric field respectively. Note that it takes approximately 106 ns to connect the two electrodes and form a discharge channel. Once the streamer reaches the opposite electrode, the electron density increases dramatically to complete the streamer-to-spark transition. However, after a few nanoseconds, the electron density and  $E/N$  decreased quickly. Subsequently, the channel shrinks, and the spark discharge extinguishes. For a long timescale, the 2D model is computationally expensive and time-consuming; therefore, the 0D model is constructed for this case. We chose a detailed chemical kinetic scheme, including 62 species and 718 chemical reactions. The discharge cycle between the two pulses was 3934 ns and the initial electron density was  $10^{12} \text{ cm}^{-3}$ . Other initial species densities are as follows:  $[N_2] = 2.60 \times 10^{18}$ ,  $[O_2] = 4.25 \times 10^{17}$ ,  $[O] = 3.83 \times 10^{17}$ ,  $[O(^1D)] = 5.88 \times 10^9$ ,  $[O_3] = 9.87 \times 10^{14}$ ,  $[O^-] = 5.23 \times 10^9$ ,  $[O_3^-] = 1.20 \times 10^8 \text{ (cm}^{-3}\text{)}$ . Subsequently, a four-layer DNN was developed and used for the case. The structure of the network is illustrated in Figure 7a. The built DNN was trained with different numbers of hidden nodes to determine the best parameters for the model performance. The number of neurons in the three hidden layers was 400, 256, and 256 respectively. The learning rate of the Adam optimiser was 0.001, and the number of training samples in each batch was 512. The evolution of loss functions with the number of epochs is shown in Figure 7b. The training converges in 100–120 epochs for the case. DeePlasKin was used to reconstruct  $E/N$  based on the electron density, and the reconstructed  $E/N$  is shown by the red line in Figure 8a, where the green line is the voltage calculated by  $E/N$ . The voltage was then used to solve the 2D discharge system. The 2D code produced a temporal evolution of electron density similar in value and trends to the benchmark in Figure 8b. In this case, we

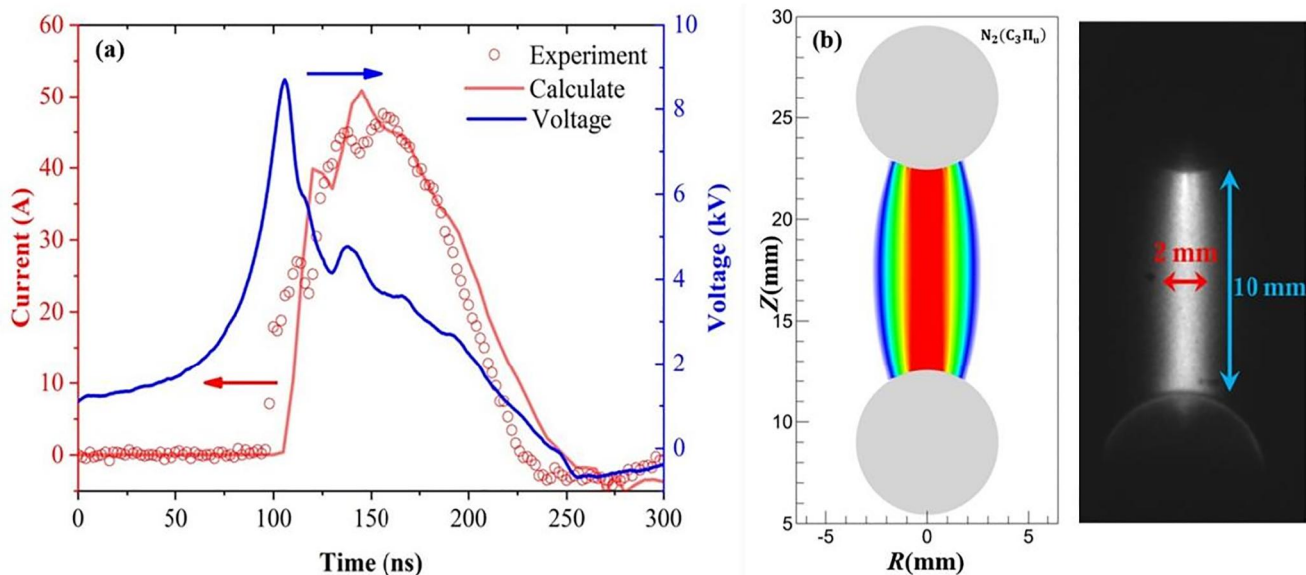


FIGURE 5 Validation of 2D model with the spark discharge experiment. (a) Comparison of calculated and experimental current [39]. (b) Comparison of the calculated and experimental  $N_2(C^3\Pi_u)$  by ICCD imaging technique [49].

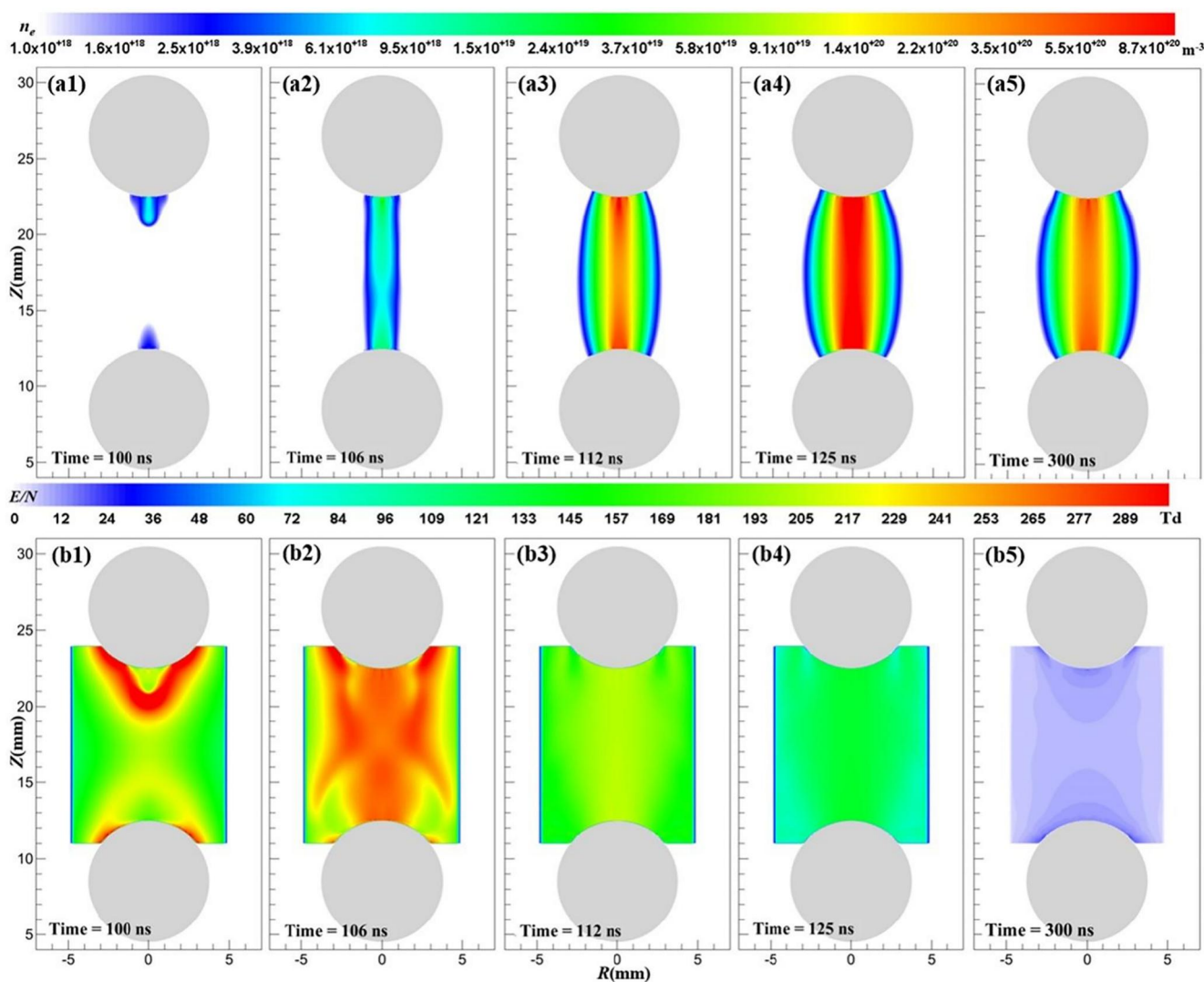


FIGURE 6 Special-temporal evolution of electron density (a1)–(a5) and reduced electric field (b1)–(b5).

considered that 30% of the discharge power was used for heating in the plasma channel (the channel radius was 1 mm), and a 2D model was constructed to calculate the neutral

molecular number density. The temporal evolution of the molecular number density is shown in Figure 9 within 500 ns. The results indicate that the pulse duration is much smaller than the

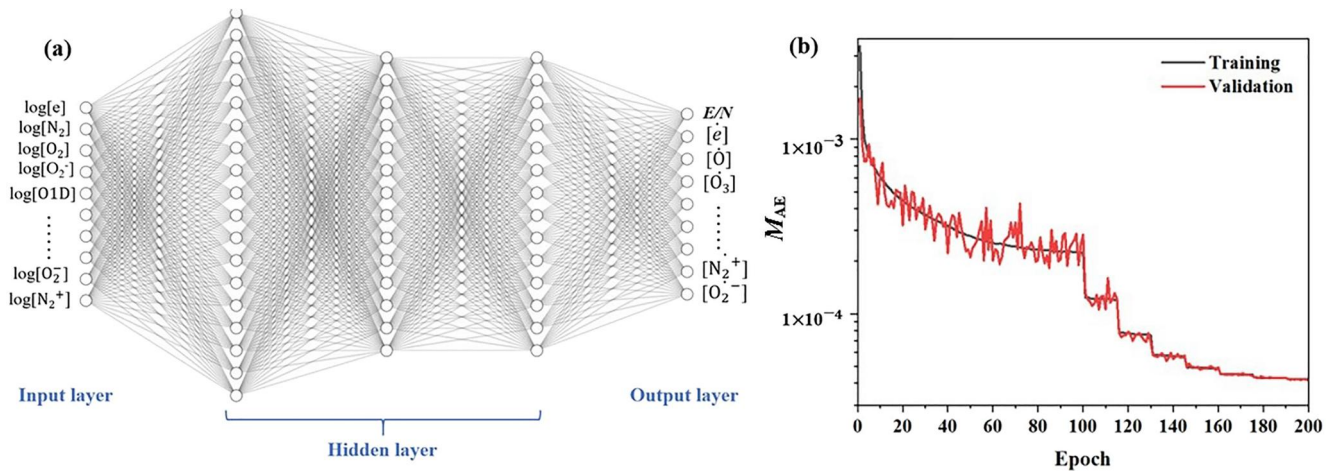


FIGURE 7 (a) Scheme of deep neural network built for air discharge. (b) Mean absolute error of training and validation.

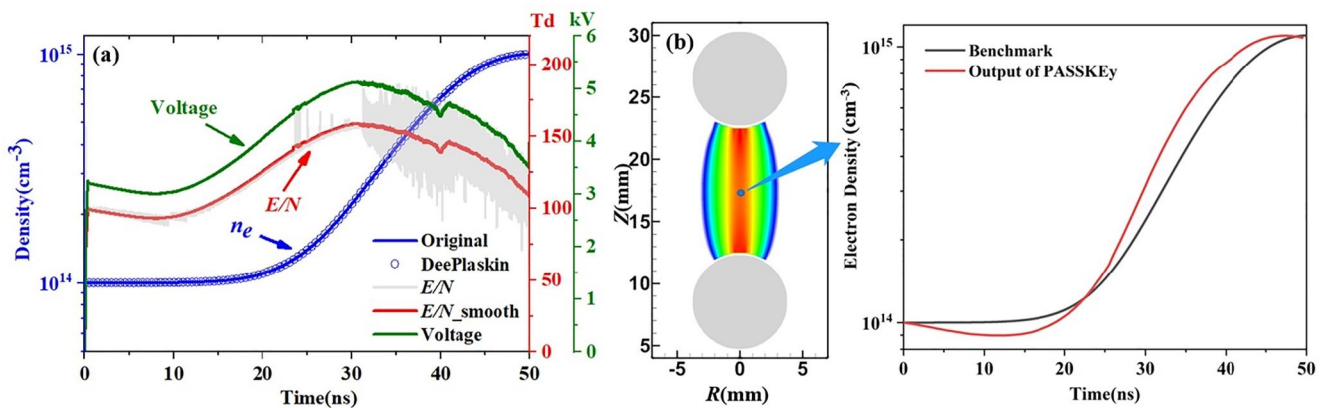


FIGURE 8 (a) Reconstructing reduced electric field and voltage by the DeePlaskin. (b) Voltage is put into the 2D model to validate the electron density.

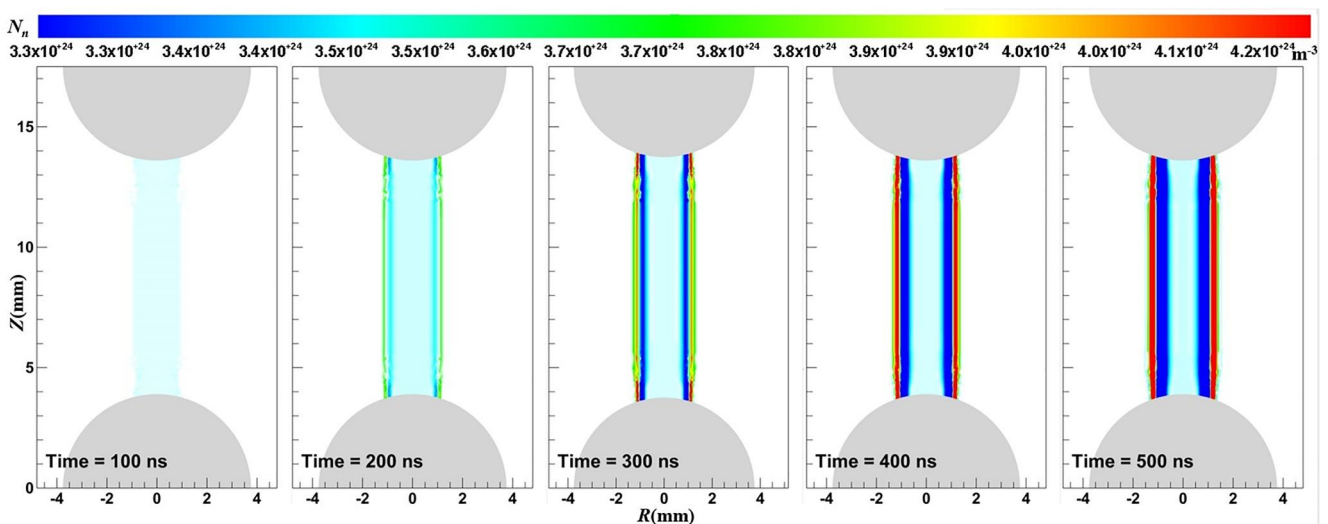


FIGURE 9 Temporal evolution of the neutral molecular number density.

gas expansion time at the three frequencies; therefore, the gas expansion does not affect the plasma parameters. In this case, the evolution of the plasma parameters during the current pulse can be simulated in the approximation of a constant gas density.

### 3.2 | Modulating sparks with regard to the pulse frequency

Repetitive frequency pulse spark discharge can produce reliable and continuous thermal and chemical effects, where the frequency and amplitude are key parameters for regulating the spark discharge. We used DeePlasKin to regulate the amplitude based on a pre-defined frequency. For the pin discharge, we chose three frequencies  $f_1 = 1/t_1 = 3.12$ ,  $f_2 = 1/t_2 = 2.631$ ,  $f_3 = 1/t_3 = 2.15$  MHz to design the voltage amplitudes shown in Figure 10. Different initial electron densities ( $1 \times 10^{14}$  cm $^{-3}$ ,  $8 \times 10^{13}$  cm $^{-3}$ ,  $6 \times 10^{13}$  cm $^{-3}$ ) correspond to the three frequencies. We used Gaussian functions to quickly increase the electron density to  $1 \times 10^{15}$  cm $^{-3}$  such that the spark discharge can be maintained in the next pulse. The voltages were calculated using DeePlasKin based on the electron densities in Figure 10I–III.

As shown in Figure 10I–III, the amplitudes are 5.12, 5.22, and 5.30 kV, respectively and  $E/N$  is 110–180 Td. The change in peak voltage from 5.12 to 5.30 kV is relatively small (an increase of 3%), while the change in the studied frequency from 2.15 to 3.12 MHz represents a substantial increase of 50%. Because in

this study varying initial values of electron density were associated with different frequencies, but the change in electron density was primarily due to differences in attenuation over time rather than significant changes in the electric field. The streamer-to-spark transition process is fast when  $E/N$  is larger than 120 Td, and if  $E/N$  is larger than 240 Td the spark will be transformed into an arc within a few nanoseconds. The designed amplitudes can maintain the spark discharge. The heating is weak at low pressure and on a small-time scale, and the influence of gas expansion can be avoided. Therefore, we can modulate the sparks to produce the required active species with respect to the pulse frequency using DeePlasKin.

### 3.3 | Modulating sparks based on species increasing mode

To achieve repeatable and energy-efficient spark discharge, we designed four modes of increasing electron density to modulate the spark during one pulse, as shown in Figure 11a. The electron density increases to the same value ( $1 \times 10^{15}$  cm $^{-3}$ ) but in four different ways: (1) Gaussian function. (2) A piecewise function in a step based on the logarithm of the electron density. (3) A linear function based on the logarithm of electron density. (4) A quadratic function based on the logarithm of the electron density. The reduced electric fields were reconstructed based on the electron densities by DeePlasKin, as shown in Figure 11b. It is quite interesting to find that, although the generated electron

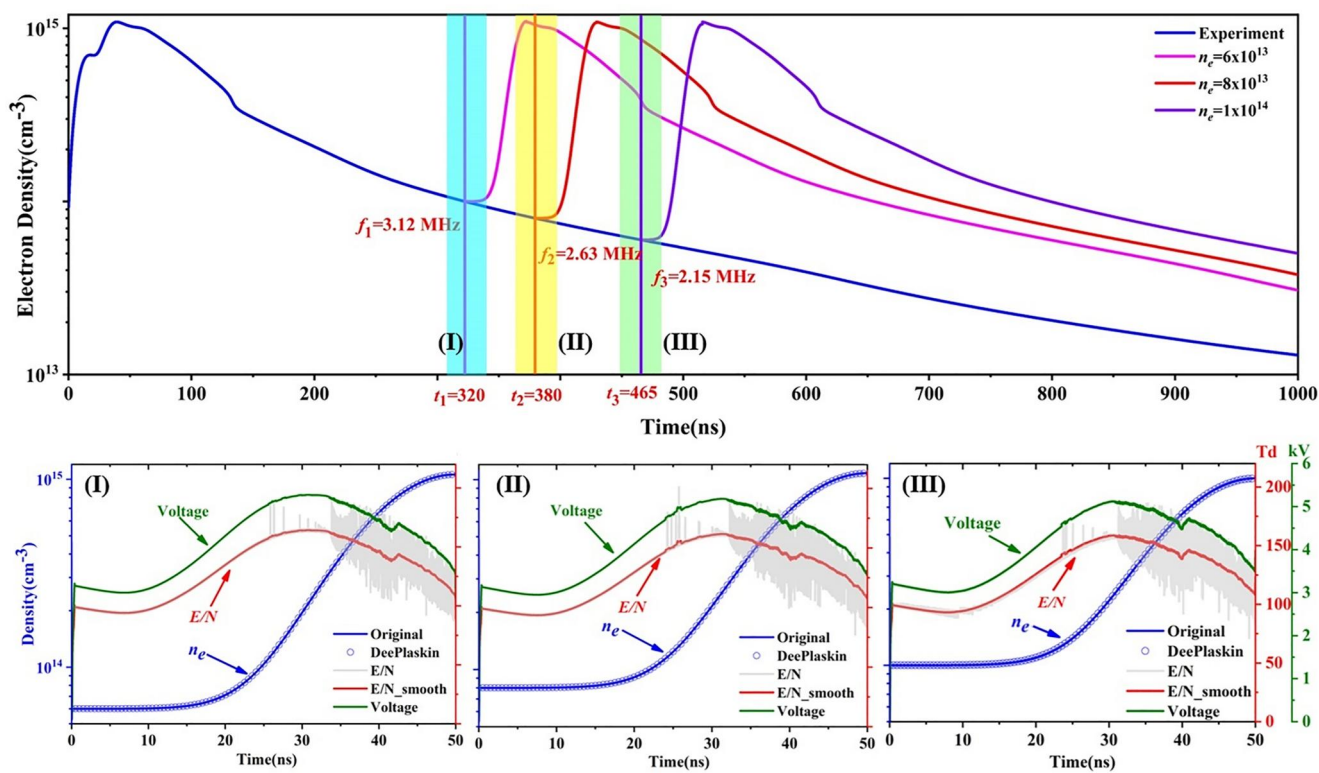


**FIGURE 10** Temporal evolution of the electron density that we design at three frequencies ( $f_1$ ,  $f_2$ ,  $f_3$ ). The calculated voltage waveform and amplitude based on their electron densities by DeePlasKin (I)–(III).

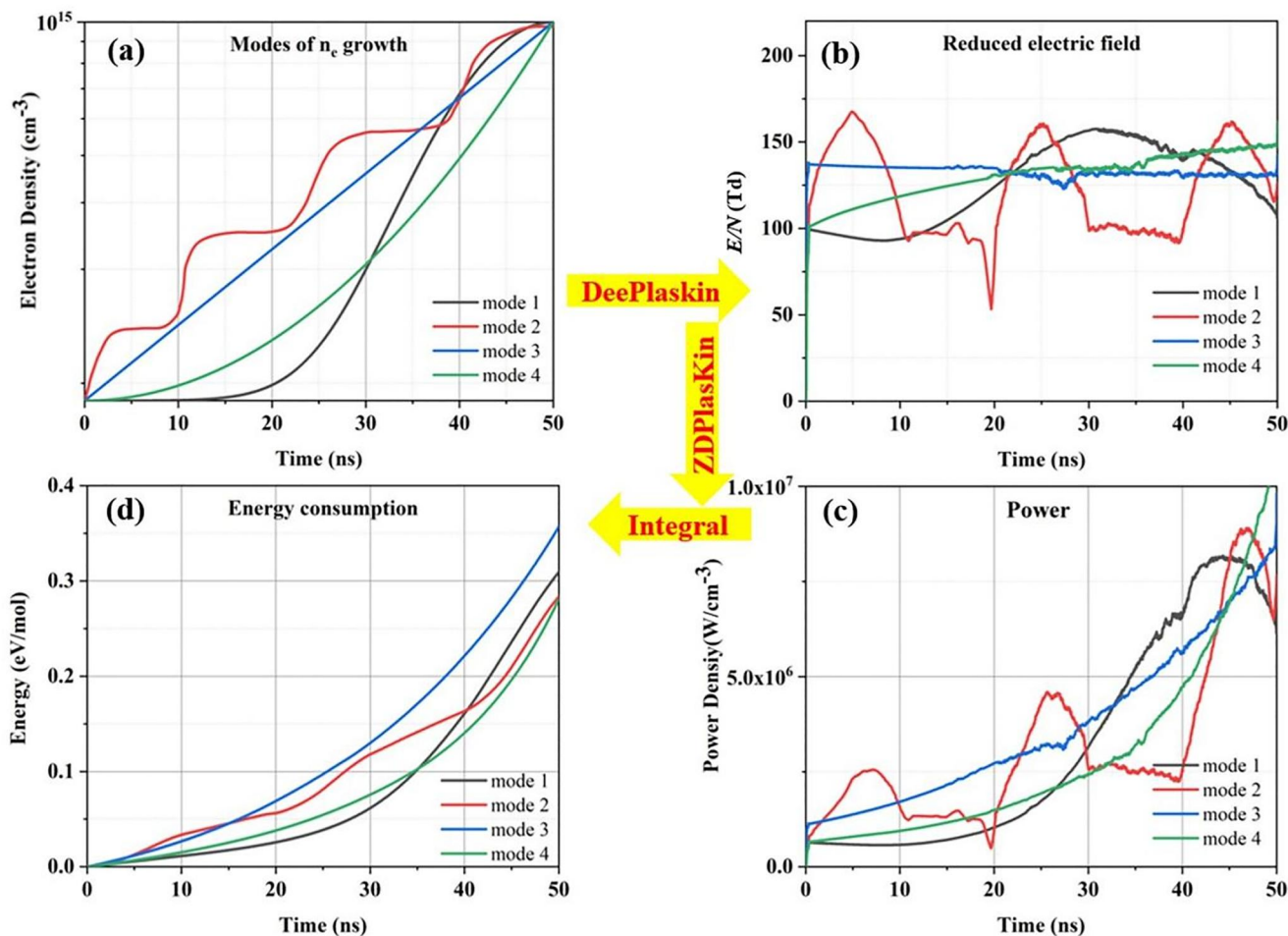


**FIGURE 11** (a) Four increasing modes of electron density. (b) Solved reduced electric field by DeePlasKin based on electron density. (c) Solved power density by ZDPlasKin based on reduced electric field. (d) Integrated energy of a molecule by power density.

densities at 50 ns are the same, the  $E/N(t)$  profile reconstructed by DeePlasKin differs. And by producing the electron density in a stepwise way, weaker but more field pulses are required. The power density ( $\text{W}/\text{cm}^3$ ) was calculated by ZDPlasKin in Figure 11c. The energy consumed (eV/mol) by a single molecule under the time integration of power density is shown in Figure 11d, and they are 0.301, 0.284, 0.357, and 0.282 eV/mol respectively. The results demonstrate that the quadratic and piecewise growth of electron density is more energy efficient, and the specific deposited energy is decreased by 5%–20% compared to other increasing modes. These facts indicate that, the energy cost to produce certain species can be reduced significantly through a strong pulse.

### 3.4 | Influence of pulse profiles on species production

For the spark discharge, we consider not only the energy consumption but also the species production. The high-energy electrons, ions, and excited particles generated by plasma

discharge can effectively split the hydrocarbon fuel into small molecules, which not only enhances the chemical activity of fuel molecules but also improves the transport effects. Ju [56] found that an O atom can significantly improve the flame stability and broaden the flammable limit. Yan [57] revealed that two chain branching and propagation reactions via direct  $\text{O}(^1\text{D})$  insertion are major pathways for radical production. Ombrello [58] found that the branching reaction of  $\text{O}_2(a^1\Delta_g)$  with H provided O and OH early in the reaction zone and increased the chemical heat release and flame propagation enhancement. However, some species play a negative role (NO and  $\text{NO}_2$  pollute the environment). The temporal evolution of these species varied with different pulse profiles, as shown in Figure 11b. The temporal evolution of O,  $\text{O}(^1\text{D})$ ,  $\text{O}_2(a^1\Delta_g)$  is shown in Figure 12a–c. The second and third modes can generate more O-atoms,  $\text{O}(^1\text{D})$  and  $\text{O}_2(a^1\Delta_g)$ , but they can generate higher densities of NO and  $\text{NO}_2$  than the fourth mode shown in Figure 12d. Under comprehensive consideration, the voltage pulse waveform corresponding to the piecewise growth of the electron density is better than the energy consumption and active species densities.

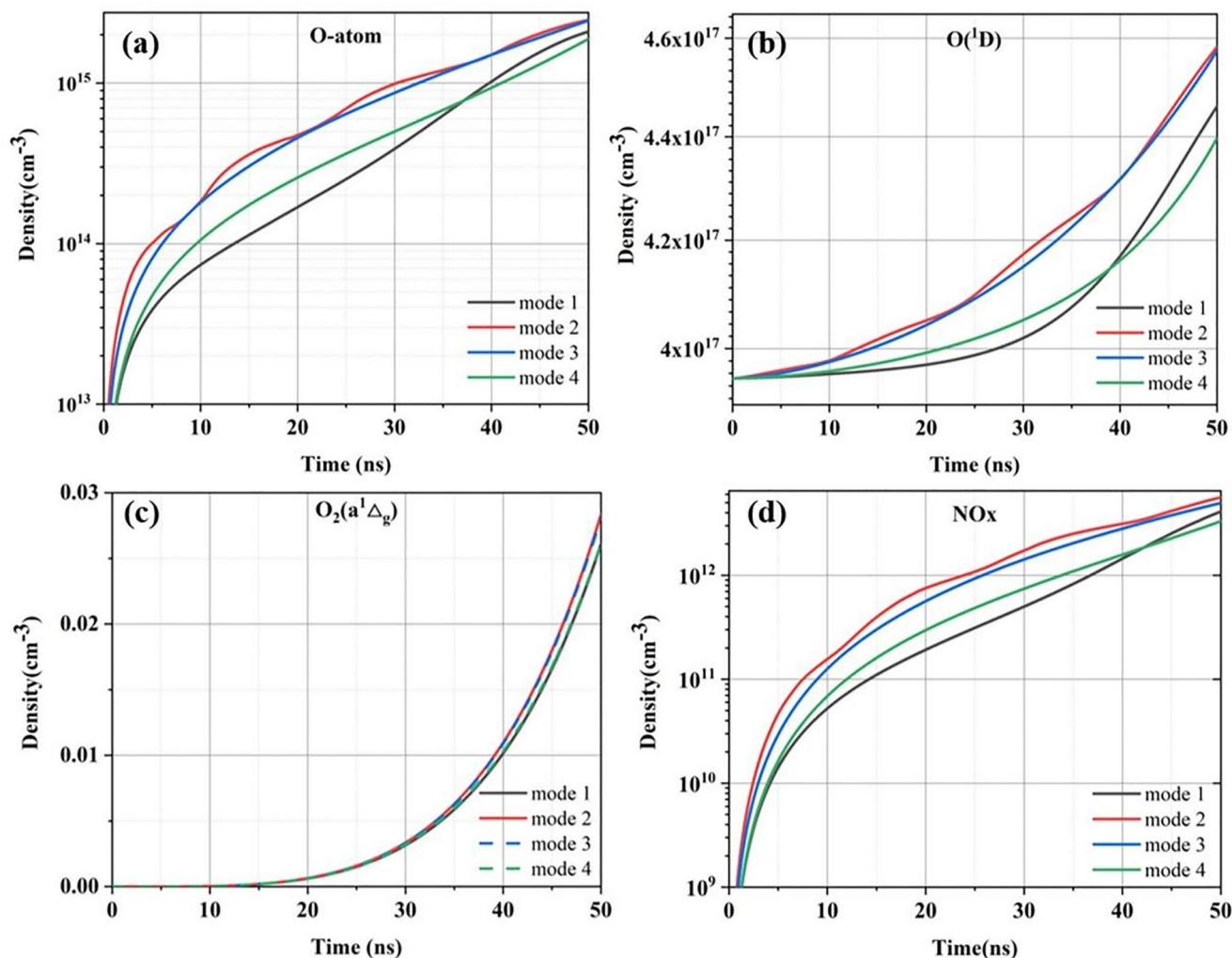


**FIGURE 12** Temporal evolution of some significant species with the different voltage waveform (corresponding to Figure 11b) for the spark discharge. (a) Temporal evolution of O-atom. (b) Temporal evolution of O( $^1D$ ). (c) Temporal evolution of O $_2(a^1\Delta_g)$ . (d) Temporal evolution of NO $_x$ .

## 4 | CONCLUSION

A repeatable and energy-efficient plasma source is required for industrial applications. The high-energy deposition and rich chemical activity of spark discharge plasmas have attracted increasing attention. The spark generated by a pulse train is a promising plasma source for highly efficient active species production and heating. By compressing a few or tens of pulses within the time scale of the gas dynamics in one periodic cycle, the influence of gas expansion on the reduced electric field can be avoided. Thus, we can modulate each pulse in the train to generate highly repeatable sparks and control the density of useful active species in a smart and energy-efficient manner.

In this study, we use a 2D model, 0D model, and physics-corrected plasma + deep learning model to modulate the profile of each pulse and automatically determine the relationship between the voltage pulse amplitude and frequency. The capabilities of the three models were confirmed using both benchmark simulation cases and experimental measurements. Good agreement was achieved between the results

obtained from the three models and the experiment for the air discharge on a time scale of 50 ns.

In addition, based on DeePlaskin, we designed four  $E/N$  profiles to simultaneously produce the same electron density simultaneously following different increasing modes. It was found that the quadratic growth of the electron density is more energy efficient, and the specific deposited energy consumption is decreased by 5%–20% compared with the other increasing modes. The voltage pulse waveform corresponding to the segmented increasing electron density was selected by comparing the energy consumption and active species densities.

Note that the coupling model cannot optimise the design automatically; therefore, we need to design a curve of the species densities to predict  $E/N$ . Automatically optimising is one of the key advantages of ML in future industries, and we will present its capability by Reinforcement Learning in future studies. In addition, the comparison with experimental data would strongly support the conclusions made in this work, however the manufacture of the user defined voltage waveforms proposed in this work is extremely hard: to produce a

tailored voltage waveform within time scale of tens of nanoseconds, is still a challenging work in the community. A recent work for generating tailored voltage waveform can be found, but it is still far from the voltage proposed in this work: we have realised that, the methodology proposed in this work, despite the improve of the efficiency, cannot be put into use shortly. Thus, the next step of this work, might be to define more practical variables of power sources (e.g. the frequency, the amplitude, or the detailed circuit elements instead).

## ACKNOWLEDGEMENTS

The work is supported by the National Natural Science Foundation of China (51907204) and Natural Science Foundation of Shaanxi Province (2021JQ-358).

## CONFLICT OF INTEREST STATEMENT

The authors declare no conflicts of interest.

## DATA AVAILABILITY STATEMENT

The data that support the findings of this study are available from the corresponding author upon reasonable request.

## ORCID

Bo Yin  <https://orcid.org/0000-0002-6275-2203>

## REFERENCES

- Bruggeman, P.J., Iza, F., Brandenburg, R.: Foundations of atmospheric pressure non-equilibrium plasmas. *Plasma Sources Sci. Technol.* 26(12), 123002 (2017)
- Starikovskaia, S.M.: Plasma assisted ignition and combustion. *J. Phys. Appl. Phys.* 39(16), R265–R299 (2006)
- Starikovskaia, S.M.: Plasma-assisted ignition and combustion: nanosecond discharges and development of kinetic mechanisms. *J. Phys. Appl. Phys.* 47(35), 335001 (2014)
- Matveev, I., et al.: Non-equilibrium plasma igniters and pilots for aerospace application. In: 43rd AIAA Aerospace Sciences Meeting and Exhibit - Meeting Papers, pp. 1191 (2005)
- Wu, Y., Li, Y.: Progress in research of plasma-assisted flow control, ignition and combustion. *High Volt. Eng.* 40(7), 2024–2038 (2014). (in Chinese)
- Liu, Z., et al.: Modulation of driving signals in flow control over an airfoil with synthetic jet. *Chin. J. Aeronaut.* 33(12), 3133–3148 (2020)
- Zhu, Y., et al.: Modelling of plasma aerodynamic actuation driven by nanosecond SDBD discharge. *J. Phys. D Appl. Phys.* 46(35), 355205 (2013)
- Tendero, C., et al.: Atmospheric pressure plasmas: a review. *Spectrochim. Acta Part B Atom. Spectrosc.* 61(1), 2–30 (2006)
- Chu, P.K., et al.: Plasma-surface modification of biomaterials. *Mater. Sci. Eng. R Rep.* 36(5–6), 143–206 (2002)
- Chen, S., et al.: Mechanism on improved surface flashover performances in vacuum of epoxy resin using fluorocarbon plasma treatment. *High Volt.* 7(3), 420–428 (2022)
- Liang, H., Ming, F., Alshareef, H.N.: Applications of plasma in energy conversion and storage materials. *Adv. Energy Mater.* 8(29), 1801804 (2018)
- Fridman, A.: *Plasma Chemistry*. Cambridge University Press (2008)
- Zhang, S., et al.: Dry reforming of methane by microsecond pulsed dielectric barrier discharge plasma: optimizing the reactor structures. *High Volt.* 7(4), 718–729 (2022)
- Yan, K., et al.: A high-voltage pulse generator for corona plasma generation. *IEEE Trans. Ind. Appl.* 38(3), 866–872 (2002)
- He, D., et al.: A novel high-voltage solid-state switch based on the SiC MOSFET series and its overcurrent protection. *High Volt.* 8(4), 698–706 (2023)
- Lorenz, S., et al.: Pulse train ignition with passively Q-switched laser spark plugs. *Int. J. Engine Res.* 17(1), 139–150 (2016)
- Chen, Z., et al.: Closing performances of double-gap laser-triggered vacuum switch. *High Volt.* 6(2), 328–336 (2021)
- Hu, Z.Y., et al.: A review of multi-physical fields induced phenomena and effects in spark plasma sintering: fundamentals and applications. *Mater. Des.* 191, 108662 (2020)
- Zhang, P., et al.: Large-scale plasma grafts voltage stabilizer on hexagonal boron nitride for improving electrical insulation and thermal conductivity of epoxy composite. *High Volt.* 8(3), 550–559 (2023).
- Minesi, N., et al.: Fully ionized nanosecond discharges in air: the thermal spark. *Plasma Sources Sci. Technol.* 29(8), 085003 (2020)
- Zhao, Z., et al.: Periodical discharge regime transitions under long-term repetitive nanosecond pulses. *Plasma Sources Sci. Technol.* 31(4), 045005 (2022)
- Korolov, I., et al.: Energy efficiency of voltage waveform tailoring for the generation of excited species in RF plasma jets operated in He/N<sub>2</sub> mixtures. *Plasma Sources Sci. Technol.* 30(9), 095013 (2021)
- Bischoff, L., et al.: Experimental and computational investigations of electron dynamics in micro atmospheric pressure radio-frequency plasma jets operated in He/N<sub>2</sub> mixtures. *Plasma Sources Sci. Technol.* 27(12), 125009 (2018)
- Korolov, I., et al.: Control of electron dynamics, radical and metastable species generation in atmospheric pressure RF plasma jets by Voltage Waveform Tailoring. *Plasma Sources Sci. Technol.* 28(9), 094001 (2019)
- Brunton, S.L., Noack, B.R., Koumoutsakos, P.: Machine learning for fluid mechanics. *Annu. Rev. Fluid Mech.* 52(1), 477–508 (2020)
- Yu, J., Hesthaven, J.S.: Flowfield reconstruction method using artificial neural network. *AIAA J.* 57(2), 482–498 (2019)
- Zhang, T., Sun, W., Ju, Y.: Multi-scale modeling of detonation formation with concentration and temperature gradients in n-heptane/air mixtures. *Proc. Combust. Inst.* 36(1), 1539–1547 (2017)
- Chen, Z.X., et al.: Application of machine learning for filtered density function closure in MILD combustion. *Combust. Flame* 225, 160–179 (2021)
- Gourisaria, M.K., et al.: Data science appositeness in diabetes mellitus diagnosis for healthcare systems of developing nations. *IET Commun.* 16(5), 532–547 (2022)
- Wu, L., Luo, X., Xu, Y.: Using convolutional neural network for diabetes mellitus diagnosis based on tongue images. *J. Eng.* 2020(13), 635–638 (2020)
- Jumper, J., et al.: Highly accurate protein structure prediction with AlphaFold. *Nature* 596(7873), 583–589 (2021)
- Zhang, P., et al.: Prediction of protein subcellular localization based on microscopic images via multi-task multi-instance learning. *Chin. J. Electron.* 31(5), 888–896 (2022)
- Xie, Y., et al.: Early lung cancer diagnostic biomarker discovery by machine learning methods. *Transl. Oncol.* 14(1), 100907 (2021)
- Saito, R., et al.: Diagnostic significance of plasma lipid markers and machine learning-based algorithm for gastric cancer. *Oncol. Lett.* 21(5), 1–8 (2021)
- Matos, F.A., Ferreira, D.R., Carvalho, P.J.: Deep learning for plasma tomography using the bolometer system at JET. *Fusion Eng. Des.* 114, 18–25 (2017)
- Kates-Harbeck, J., Svyatkovskiy, A., Tang, W.: Predicting disruptive instabilities in controlled fusion plasmas through deep learning. *Nature* 568(7753), 526–531 (2019)
- Liu, H., et al.: A deep-learning-based method for diagnosing time-varying plasma adopting microwaves. *IEEE Trans. Plasma Sci.* 49(4), 1406–1413 (2021)
- Mathews, A., et al.: Uncovering turbulent plasma dynamics via deep learning from partial observations. *Phys. Rev. E* 104(2), 025205 (2021)
- Van Der Gaag, T., Onishi, H., Akatsuka, H.: Arbitrary EEDF determination of atmospheric-pressure plasma by applying machine learning to OES measurement. *Phys. Plasmas* 28(3), 033511 (2021)

40. Kawaguchi, S., et al.: Deep learning for solving the Boltzmann equation of electrons in weakly ionized plasma. *Plasma Sources Sci. Technol.* 29(2), 025021 (2020)
41. Mesbah, A., Graves, D.B.: Machine learning for modeling, diagnostics, and control of non-equilibrium plasmas. *J. Phys. D Appl. Phys.* 52(30), 30LT02 (2019)
42. Zhong, L., Gu, Q., Wu, B.: Deep learning for thermal plasma simulation: solving 1-D arc model as an example. *Comput. Phys. Commun.* 257, 107496 (2020)
43. Zhang, Y., et al.: Physics-informed deep neural network for inhomogeneous magnetized plasma parameter inversion. *IEEE Antenn. Wireless Propag. Lett.* 21(4), 828–832 (2022)
44. Zhu, Y., et al.: Tailoring electric field signals of nonequilibrium discharges by the deep learning method and physical corrections. *Plasma Process. Polym.* 19(3), e2100155 (2022)
45. Pancheshnyi, S., et al.: ZDPlasKin: a new tool for plasmachemical simulations. *APS Meet. Abstr.* 53 (2008)
46. Zhu, Y., et al.: Nanosecond-pulsed dielectric barrier discharge-based plasma-assisted anti-icing: modeling and mechanism analysis. *J. Phys. D Appl. Phys.* 53(14), 145205 (2020)
47. Zhu, Y., et al.: Simulation of ionization-wave discharges: a direct comparison between the fluid model and E-FISH measurements. *Plasma Sources Sci. Technol.* 30(7), 075025 (2021)
48. Shkurenkov, I., Adamovich, I.V.: Energy balance in nanosecond pulse discharges in nitrogen and air. *Plasma Sources Sci. Technol.* 25(1), 015021 (2016)
49. Montello, A., et al.: Picosecond CARS measurements of nitrogen vibrational loading and rotational/translational temperature in non-equilibrium discharges. *J. Phys. Appl. Phys.* 46, 464002 (2013)
50. Chen, X., Zhu, Y., Wu, Y.: Modeling of streamer-to-spark transitions in the first pulse and the post discharge stage. *Plasma Sources Sci. Technol.* 29(9), 095006 (2020)
51. Hagelaar, G.J.M., Pitchford, L.C.: Solving the Boltzmann equation to obtain electron transport coefficients and rate coefficients for fluid models. *Plasma Sources Sci. Technol.* 14(4), 722–733 (2005)
52. Zhu, Y., et al.: Optical actinometry of O-atoms in pulsed nanosecond capillary discharge: peculiarities of kinetics at high specific deposited energy. *Plasma Sources Sci. Technol.* 27(7), 075020 (2018)
53. Wibawa, M.S.: Pengaruh Fungsi Aktivasi, Optimisasi dan Jumlah Epoch Terhadap Performa Jaringan Saraf Tiruan. *Jurnal Sistem dan Informatika* 11(2), 075020 (2017)
54. Zhang, Z.: Improved adam optimizer for deep neural networks. In: 2018 IEEE/ACM 26th International Symposium on Quality of Service, IWQoS, pp. 1–2 (2018)
55. Marcham, F.: TensorFlow: large-scale machine learning on heterogeneous distributed systems (preliminary white paper, November 9, 2015). *Library s4-X(3)*, 339 (1929)
56. Ju, Y.: Recent progress and challenges in fundamental combustion research. *Adv. Mech.* 44(1), 21–83 (2014)
57. Yang, W., et al.: When machine learning meets multiscale modeling in chemical reactions. *J. Chem. Phys.* 153(9), 094117 (2020)
58. Ombrello, T., et al.: Flame propagation enhancement by plasma excitation of oxygen. Part II: effects of O<sub>2</sub>(a1Δg). *Combust. Flame* 157(10), 1916–1928 (2010)

**How to cite this article:** Yin, B., Zhu, Y., Wu, Y.: Modulating sparks in a pulse train for repetitive and energy efficient plasma generation. *High Voltage.* 8(6), 1168–1179 (2023). <https://doi.org/10.1049/hve2.12348>